# Analysis of Optical Absorbance Spectra for the Determination of ZnO Nanoparticle Size Distribution, Solubility, and Surface Energy

**Doris Segets, Johannes Gradl, Robin Klupp Taylor, Vassil Vassilev, and Wolfgang Peukert***

Institute of Particle Technology, Friedrich-Alexander-University Erlangen-Nuremberg, Cauerstr. 4, 91058 Erlangen, Germany

**ABSTRACT** We present a model to calculate particle size distributions (PSDs) of colloidal ZnO nanoparticles from their absorbance spectra. Using literature values for the optical properties of bulk ZnO and correlating the measurement wavelengths in the UV—visible regime with distinct particle sizes by a tight binding model (TBM), an algorithm deconvolutes the absorbance spectra into contributions from size fractions. We find an excellent agreement between size distributions determined from TEM images and the calculated PSDs. For further validation, bimodal PSDs have been investigated and an approach to determine not only particle size but also solid concentration is introduced. We will show the applicability of our model by the determination of temperature-dependent ripening rates, which enables the calculation of solubilities, surface tensions, and the activation enthalpy of ripening. In principle, our methodology is applicable to different semiconductor nanoparticles in various solvents as long as their bulk properties are known and scattering is negligible.

**KEYWORDS:** ZnO nanoparticles · absorbance · particle size distribution · ripening rates · solubility

The synthesis and characterization of ZnO nanoparticles has found widespread interest during the past 10 years due to their unique electro-optical properties.[1−3] For instance, ZnO nanoparticles were recently functionalized with charge transfer complexes, such as porphyrins, and the charge transfer for the dye molecules and the nanoparticles was studied in detail.[4] However, the reproducible, noninvasive determination of small particle sizes in the sub-10 nm range remains an important and challenging task. In most cases, the quantum size effect (*e.g.*, the blue shift of the absorption edge of semiconductor nanoparticles[5] with decreasing particle size) is used, for example, to determine slow ripening kinetics[6−8] or to investigate nanoparticle growth.[9,10] In several cases, the particle size is determined from the effective mass approximation (EMA) derived by Brus.[11] Since this approach only allows a rough estimation of the real particle size, Viswanatha *et al.*[12] showed that the EMA breaks down for particle sizes below 5 nm. Furthermore, the calculation of a mean particle diameter taking the onset of an absorption edge only provides a rough estimation and will never give the whole PSD. In contrast, Pesika *et al.*[13] developed a model to determine PSDs using the slope between the onset and the maximum of the investigated spectrum based on the EMA. This description is more accurate than just considering one single wavelength, but information is lost by neglecting absorbance information at wavelengths shorter than the peak wavelength. Nevertheless, to the best of our knowledge, there are no further approaches in the literature that provide access to a PSD from optical absorbance. In this paper, we introduce a new model for calculating PSDs from absorbance spectra using information from the whole spectrum. By means of a tight binding model (TBM) from Viswanatha, we correlate the measurement wavelengths with different particle sizes. Furthermore, our considerations are based on the optical properties of bulk ZnO.[14,15] We validate our model and compare the results with other measurement techniques to determine PSDs, including dynamic light scattering (DLS) and transmission electron microscopy (TEM). In a further step, our model has been extended to the calculation of solid concentration. Finally, the determination of temperature-dependent ripening rates enables the calculation of the activation energy of ripening and the determination of widely unknown solubility data of ZnO in ethanol. Therefore, mean solubilities and macroscopic surface energies are calculated without assuming any thermodynamic materials data.

*Address correspondence to w.peukert@lfg.uni-erlangen.de.

Received for review March 6, 2009 and accepted May 20, 2009.

**Published online June 9, 2009.**
10.1021/nn900223b CCC: $40.75

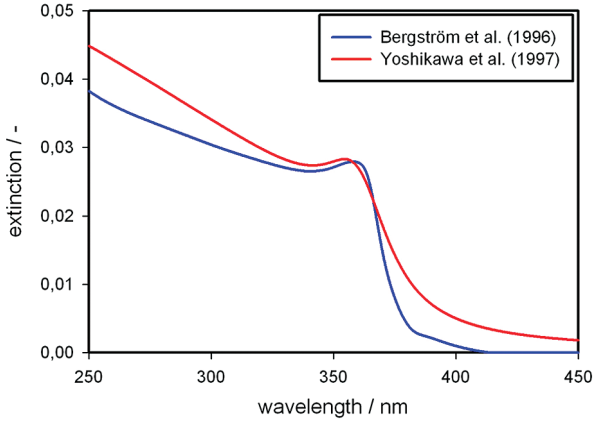


**Figure 1. Absorbance of bulk ZnO according to Bergström (blue line) and Yoshikawa (red line).**

## THEORETICAL FRAMEWORK

The determination of a PSD from an absorbance spectrum is based on the fact that the optical properties of small semiconductor quantum dots, such as ZnO nanoparticles, depend on their disperse properties, namely, size and shape. The challenge thereby is to find an appropriate description for this relation because the overall extinction is not only influenced by the absolute particle concentration according to Lambert−Beer's law at sufficiently low concentrations but the absorption coefficient is also a function of particle size. Accordingly, the model consists of two aspects. First, we obtained two sets of literature values for the bulk complex dielectric function of ZnO thin films as determined by spectroscopic ellipsometry by Yoshikawa[14] and Bergström.[15] These were then converted into absorption coefficient spectra. Figure 1 shows the comparison of the absorption spectra of bulk ZnO between 250 and 400 nm according to both authors. Apparently, both approaches lead almost to the same position of the peak, but there is a strong deviation between their results regarding the remaining spectrum. Therefore, in the following, we always denote which model was used.

The second stage of our treatment considers the quantum size effect. Due to the small dimensions of semiconductor nanoparticles, a discretization of the band gap occurs with decreasing particle size, leading to smaller excitation frequencies. A blue shift is observed in the extinction behavior, and the absorption edge is positioned at smaller wavelengths. We assume that the absorbance of small nanoparticles in principle remains unchanged but is parallel shifted to smaller wavelengths depending on the particle diameter. The expected absorbance of different particle sizes is demonstrated in Figure 2 for three different diameters of 2.5, 5, and ≫10 nm, and both models were used to describe the bulk properties.

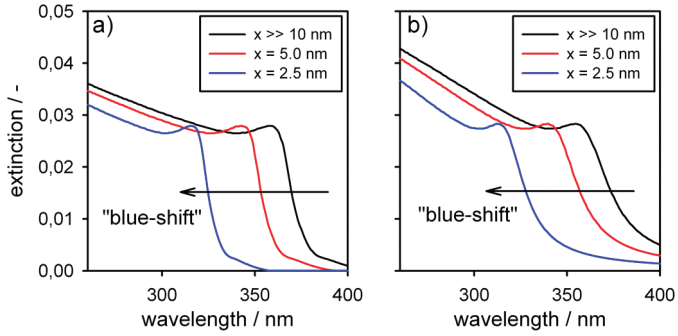


**Figure 2. (a) Theoretical absorbance of differently sized ZnO nanoparticles according to the presented model based on the bulk properties calculated by Bergström. (b) Theoretical absorbance of differently sized ZnO nanoparticles according to the presented model based on the bulk properties calculated by Yoshikawa.**

We are aware that this does not reflect the exact size-dependent absorbance behavior of very small particles. However, to the best of our knowledge, there are currently no libraries available of wavelength-dependent optical properties for monodisperse ZnO quantum dots covering the size range of interest (less than 10 nm). Furthermore, it has to be stressed that the presented model is not limited to the use of the shifted bulk data. The main issue is the decomposition of the spectra that is presented in the following, whereas the actual optical properties used are somewhat arbitrary. Therefore, if better suited optical property data sets for ZnO quantum dots are available in the future, they will be easily implemented into our approach.

For real suspensions containing not only one defined particle size but also a PSD, each particle fraction contributes to the overall spectrum according to its distinct size and relative concentration. Thus, the measured spectrum is the linear sum of all the single absorbance spectra according to

$$Q_{abs} = \sum_{x(\lambda_{min}=260nm)}^{x(\lambda_{max}=365nm)} (\alpha(x(\lambda))\cdot q_3(x(\lambda))\cdot \Delta x(\lambda)\cdot d_C) \quad (1)$$

$Q_{abs}$ is the overall absorbance of the suspension; $\lambda$ is the investigated wavelength; $x$ is the particle diameter; $\Delta x$ is the particle size difference corresponding to the discrete wavelength interval $\Delta\lambda$; $\alpha$ is the absorption coefficient; $q_3$ is the volume density distribution of the suspension, and $d_C$ is the optical path length, or the thickness of the measuring cuvette, respectively; $\lambda_{max} = 365$ nm is the absorption edge onset of the bulk material, and $\lambda_{min} = 260$ nm is the shortest wavelength that is considered. These two limits have been chosen according to the following considerations: Regarding the particle sizes which can be identified, the upper limit is determined by the absorption onset of the bulk, which is 365 nm in the case of ZnO (corresponding to 28 nm). The determination of the lower limit is more difficult. This depends on the model used to correlate certain wavelengths with particle sizes. In the present paper, this is realized *via* a tight binding model (TBM).[12] As is clear from this reference (but the same trend holds, *e.g.*, also for other models such as the effective mass approximation), the smaller the particle size the larger the

difference of the band gap between a defined particle size interval $\Delta x$. Thus, between 260 nm (which refers to 1.19 nm in particle size) and 270 nm (which refers to 1.31 nm in particle size), the difference in the correlated particle sizes is only 0.12 nm. Thus, evaluating shorter wavelengths does not bring any significant further benefit. Additionally, with sizes around 1 nm, a quantum mechanic limit is reached since the "particles" are built of only a few molecular units. Therefore, a continuous description is no longer useful.

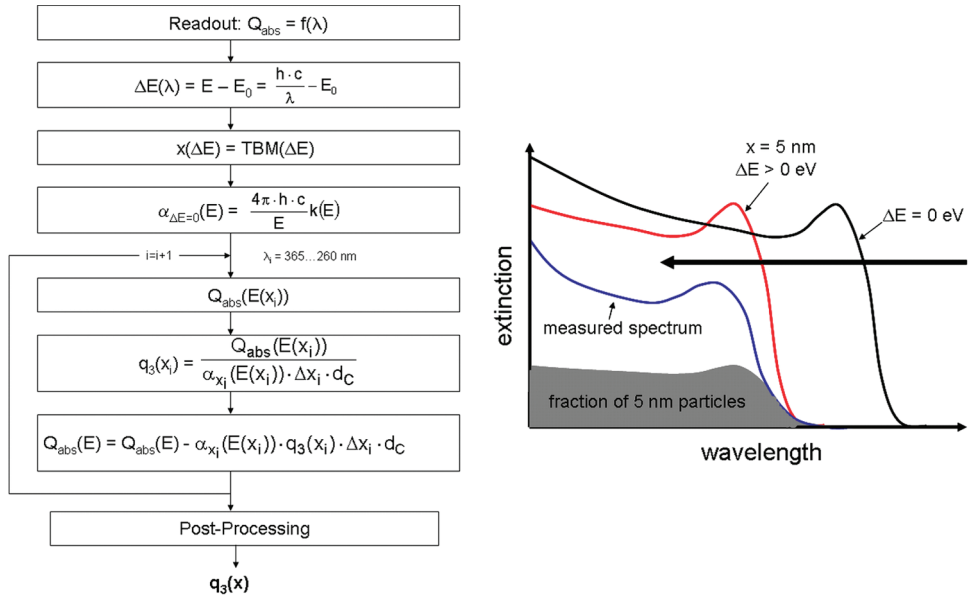


**Figure 3. Scheme of the algorithm and example of one run of its application on a measured spectrum.**

The particle diameters are derived by converting the measured wavelengths in a first step into band gap energy differences ($\Delta E$) according to

$$\Delta E(\lambda) = E - E_0 = \frac{h \cdot c}{\lambda} - E_0 \qquad (2)$$

where $E$ is the energy corresponding to the investigated wavelength $\lambda$; $E_0$ is the bulk band gap energy; $h$ is Planck's constant, and $c$ is the velocity of light. These energy differences are then correlated with different particle sizes by the TBM. The theoretical absorption behavior of the bulk phase $\alpha_{\Delta E=0}(E)$ is calculated from the data of Bergström or Yoshikawa, and the deconvolution of the measured absorbance spectrum proceeds as follows: The bulk absorbance spectrum is multiplied by the measured value of absorbance at the wavelength corresponding to the bulk absorption edge onset ($\lambda$ = 365 nm). This leads to a spectrum $Q_{abs}(E(x_i))$ that describes the size-weighted absorbance of the regarded largest particle size fraction $i$. Then, according to eq 1, the values of $Q_{abs}(E(x_i))$ are converted to a volume size fraction $q_3(x_i)$ by dividing by the value of the shifted absorption coefficient at this wavelength $\alpha_{x_i}(E(x_i))$, the thickness of the sample cuvette $d_C$, and the corresponding particle size interval $\Delta x_i$. The value of $q_3(x_i)$ corresponds to one point in the PSD. Before the next point is determined, the size-weighted absorbance spectrum $Q_{abs}(E(x_i))$ is subtracted from the measured spectrum, thus removing the absorbance contributions from the particles in the size interval $\Delta x_i$. The bulk absorbance spectrum is then blue-shifted by a discrete wavelength step, and the process of multiplication with the measured absorbance value corresponding to the new "bulk" absorption edge onset and subsequent conversion to a volume size fraction $q_3(x_{i+1})$ is repeated. This procedure continues until all parts of the measured spectrum are analyzed. Consequently, the volume density distribution $q_3(x)$ is constructed. This is achieved by normalizing the area below the distribution according to

$$\sum_{x_{min}}^{x_{max}} q_3(x) \cdot \Delta x = 1 \qquad (3)$$

A scheme of the algorithm and its application on an exemplary absorbance spectrum of ZnO is shown in Figure 3.

Finally, it has to be stressed that in its current form the algorithm is only applicable to nonscattering systems. If scattering should also be considered (*e.g.*, for larger particles), then an implementation of Mie's theory would be necessary, which would add another layer of complexity.

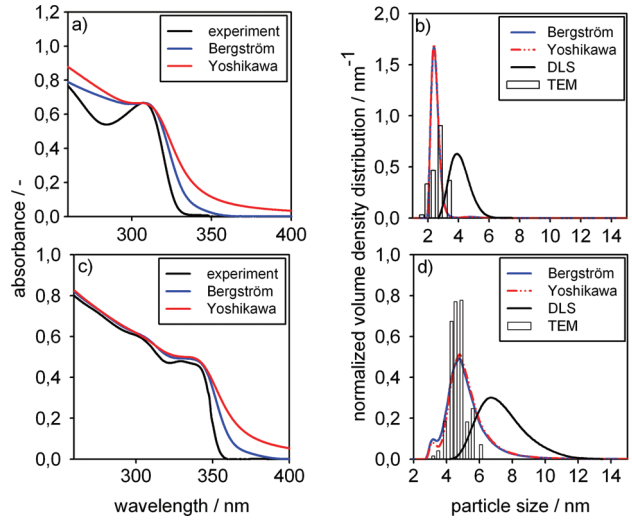


**Figure 4. Comparison between the model, DLS and optical image analysis of two different PSDs stored at (b) −10 and (d) 20 °C and the related measured and reconstructed absorbance spectra at (a) −10 and (c) 20 °C.**

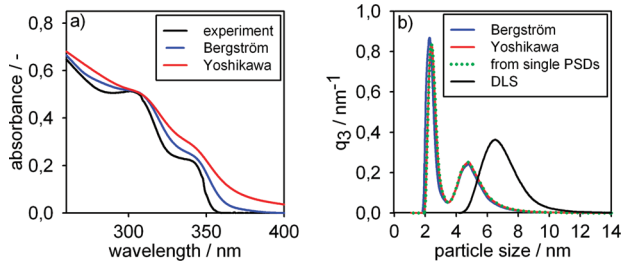


**Figure 5. (a) Absorbance spectrum of the bimodal PSD after mixing the two suspensions in the same volume ratio (black line) and its corresponding reconstructions (blue and red lines). (b) Bimodal PSD calculated from the bimodal absorbance spectrum with the bulk properties from Bergström and Yoshikawa (blue and red lines), expected bimodal PSD calculated from the PSDs of the pure unmixed suspensions (green dotted line), and bimodal PSD measured with DLS (black line).**

## RESULTS AND DISCUSSION

**Reconstruction of PSD.** Figure 4 shows the measured absorbance spectra for suspensions containing small and large particles (Figure 4a,c, respectively, black lines) and the corresponding derived and measured PSDs (Figure 4b,d). It can be seen that the absorption peak of the suspension ripened at −10 °C (Figure 4a) is positioned at wavelengths below 330 nm, whereas the absorption peak of the suspension ripened at the higher temperature of 20 °C (Figure 4c) is positioned at longer wavelengths at around 340 nm. A broadening of the peak is also observed with increased ripening temperature. Both absorbance spectra do not show a strong sharpening of the excitonic feature near the absorption edge, as in both cases this effect is smeared out due to the present polydispersity. In Figure 4b,d, a comparison is made of the PSDs obtained for both suspensions using our algorithm with the PSDs determined by DLS and TEM image analysis. It can be seen that the results of the TEM image analysis and the PSD calculated from the absorbance spectra coincide very well, whereas DLS gives somewhat larger particle sizes. This is due to the fact that, on the one hand, the resolution of our DLS measuring device for sizes below 10 nm is low and that, on the other hand, the solvent layers associated with the particles become more and more dominant with decreasing particle size. The apparent agreement of the algorithm with the TEM image analysis is a first indication that the previously taken assumptions concerning the optical properties of quantum dots are acceptable. In fact, the algorithm itself appears to be rather insensitive to whether the bulk properties are described according to the data of Yoshikawa or to Bergström. However, if we attempt to reconstruct the absorbance spectra from the previously calculated PSDs, the use of both bulk absorbance data sets results in larger discrepancies, as shown with blue and red lines in Figure 4a,c. While the characteristic peak is the same for both calculated spectra, in comparison to the measured spectra, the reconstructions using the optical bulk properties according to Bergström agree better. The measured absorbance cannot be reconstructed completely due to the fact that the assumptions made concerning the optical properties of small quantum dots are not exact as already described in the previous section. However, this indicates a potentially important validation of our method as it is possible to implement arbitrary "bulk" spectra in the algorithm and invert to see if the original measured spectrum can be obtained. In this respect, it should be possible to use optimization techniques to derive iteratively a size-dependent dielectric function for ZnO which minimizes the difference between the measured and reconstructed spectra. These optical properties could then be implemented into our model. Another possibility would be to produce highly monodisperse nanoparticles (*e.g.*, *via* the hot injection method)[16] in order to measure the absorbance spectra of different size fractions and thereby to determine experimentally the size-dependent dielectric function. However, this would go beyond the scope of the present work.

For further validation, the two suspensions were mixed in equivalent volume ratios ($V_1 = V_2$) and the absorbance of the resulting bimodal suspension was measured. Additionally, a DLS measurement was performed. Figure 5a shows the bimodal absorbance spectrum (black line) and the corresponding reconstructions from the algorithm (blue and red lines). The characteristic peaks of the pure suspensions are still reflected at $\lambda_1 = 310$ nm and $\lambda_2 = 340$ nm. In Figure 5b, the bimodal PSDs calculated out of the measured bimodal spectrum underlying the bulk properties of both Bergström and Yoshikawa are shown in blue and red lines, respectively. The green dotted line illustrates the theoretically expected bimodal curve progression calculated from the PSDs of the pure, unmixed suspensions. It can be seen that the bimodal PSDs determined from the individual volume density distributions and those derived from the bimodal absorbance spectrum agree very well, whereas the DLS measurement does not resolve any bimodality.

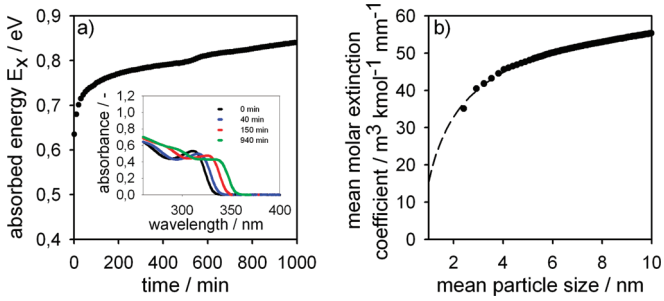


**Figure 6. (a) Size-dependent absorbed energy of a ZnO suspension ripening at 30 °C and corresponding absorbance spectra after 0, 40, 150, and 940 min (inset). (b) Mean absorption coefficient calculated for particle sizes between $x_{1,3} = 2$ nm and $x_{1,3} = 10$ nm and corresponding fit curve.**

**Determination of Solid Concentration.** Due to the good resolution of bimodal volume fractions by our algorithm, it is possible to derive information not only about

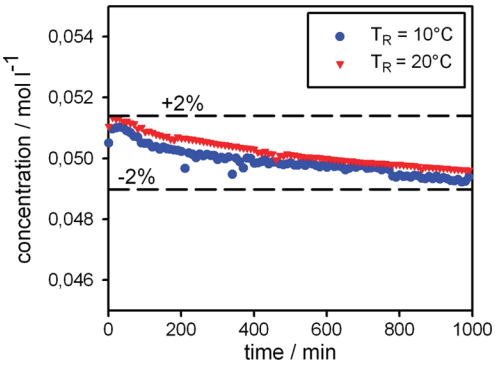


**Figure 7. Concentration during ripening at 10 °C (blue line) and 20 °C (red line); the expected solid concentration is 0.050 M.**

the PSD but also about absolute solid concentrations. However, it is necessary to correct for the fact that the mean molar extinction coefficient changes with particle size. In principle, our model contains the information on concentration as it is apparent from the evaluation of the bimodal absorbance spectra, but for the exact calculation of concentrations, it has to be kept in mind that there is always a certain deviation between the reconstructed and the measured spectra, especially in the case of small particle sizes (see Figure 4a). Therefore, the previously introduced model is extended for the determination of solid concentrations using a size-dependent mean extinction coefficient $\varepsilon$. This extinction coefficient is calculated from a ZnO suspension ripened at 30 °C over time in order to cover a broad range of particle sizes. At every point in time, a mean volume equivalent particle diameter $x_{1,3}$ is calculated with the previously introduced algorithm and the corresponding overall energy absorbed $E_x$ is determined according to

$$E_x(t) = \sum_{\lambda=260\text{nm}}^{\lambda=365\text{nm}} (Q_{abs}(\lambda)\cdot\Delta E(\lambda)) \qquad (4)$$

Assuming completion of the reaction (resulting in $c_{ZnO} = 0.05$ M) and the incorporation of all available ZnO molecules into particles, the mean size-dependent extinction coefficient is calculated for each particle size according to Lambert−Beer's Law. The absorbance spectra and the calculated energy absorbed with time are illustrated in Figure 6a, whereas Figure 6b shows the derived mean extinction coefficients for particle sizes from 2 to 10 nm. With this knowledge, the concentration of an unknown suspension can be determined from the absorbance behavior:

$$c_{ZnO} = \frac{E_x}{\varepsilon(x)\cdot d_C} \qquad (5)$$

with

$$\varepsilon\left[\frac{m^3}{\text{kmol}\cdot\text{mm}}\right] = \left[-56.8\cdot\left(\frac{x}{\text{nm}}\right)^{-0.52} + 72.4\right]\frac{m^3}{\text{kmol}\cdot\text{mm}} \qquad (6)$$

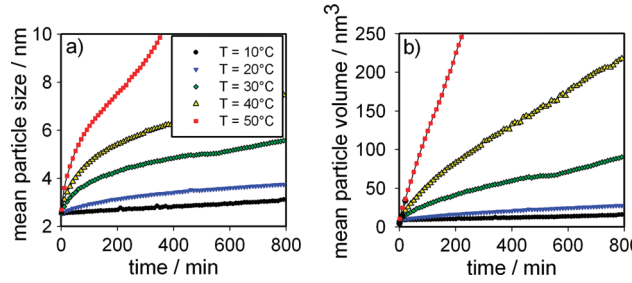


**Figure 8. (a) Influence of the temperature on the mean volume weighted particle size $x_{1,3}$. (b) Influence of the temperature on the particle volume.**

To validate this approach, the absorbance spectra of two identical ZnO suspensions originating from the same batch but ripened at different temperatures have been recorded and the solid concentrations at each point in time have been calculated (see Figure 7). Independent of their particle size distribution, both samples have the same expected concentration of 0.05 M ± 2%. With increasing ripening time, there is a slight decrease in concentration for both temperatures. One reason for this observation could be that the extinction coefficient has been determined at 30 °C under the assumption that it is independent of the temperature. However, in the case of many liquids, the extinction increases marginally with temperature due to changing interactions of the solute with the solvent molecules. Such effects are neglected for the present work as the effects are expected to be small. Now that the algorithm has been validated regarding the calculation of PSD and solid concentration, it can be used for the investigation of long-term ripening kinetics.

However, at this stage, it should be pointed out that the validation of our model is based on comparison with published data and by optical image analysis. Due to technical challenges, there is no validation of the properties of our colloids *via* a second measurement technique. For independent validation of, for example, the mass concentration, it would be necessary to separate different particle sizes from the liquid phase and to determine their optical properties as well as their concentration. Precipitation of the particles (*e.g.*, with hep-

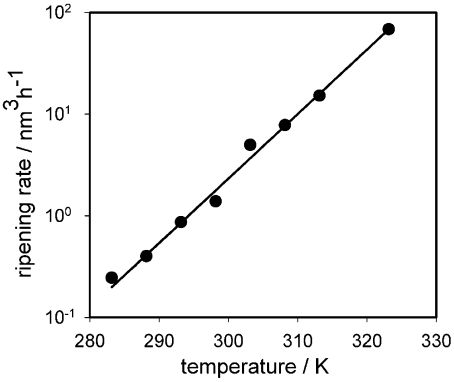


**Figure 9. Linear mean ripening rate of ZnO in ethanol for temperatures between 10 and 50 °C and correlation of the data with an Arrhenius law.**

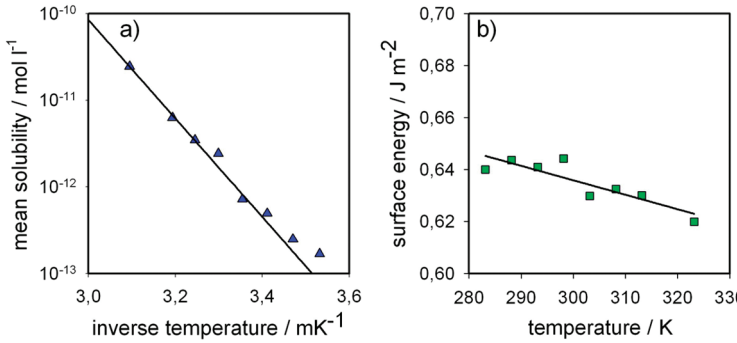


**Figure 10. (a) Temperature dependence of the global solubility. (b) Temperature dependence of the surface energy of ZnO in ethanol.**

tane) is excluded as it would change the solubilities, thus only filtration and ultracentrifugation could be applied. However, the scope of the current work is not the physicochemical investigation of small ZnO quantum dots but rather the introduction of a comparatively simple, economical, and flexible approach to determine PSD and solid concentration for semiconductor nanoparticles.

**Ripening Kinetics.** In the following, the activation energy of ripening, temperature-dependent solubilities, and surface energies are derived. The first investigations on the ripening of ZnO particles were performed by Meulenkamp and Wong,[6,8] who both applied the effective mass approximation to determine the mean particle size. During ripening, small particles are dissolving and free molecules or molecular aggregates are incorporated into larger crystal structures.[17] Therefore, a suspension of ZnO was synthesized and directly stored at −20 °C. Due to the freezing of the suspension, the optical properties were constant and the particle diameter remained unchanged ($x_{1,3}$ = 2.4 nm for several months). From this suspension, samples were taken and put into a cuvette (optical path length of 200 μm) for measurement of the temperature-dependent change of the absorbance spectra at 10 min intervals. The calculated change of the mean particle diameter $x_{1,3}$ and the corresponding change of the particle volume with time for temperatures between 10 and 50 °C are shown in Figure 8. From Figure 8a, it can be seen that with increasing temperature the particle size is growing due to an increasing solubility. The suspension measured at 50 °C was only stable during the first 380 min. Afterwards, aggregation of the particles commenced and the measurement was stopped. Regarding Figure 8b, it can be seen that after an initial nonlinear phase the increase of volume with time is constant.

Assuming diffusion-limited ripening and expressing the Gibbs−Thomson equation *via* the first two terms of a Taylor series, the change of the particle volume with time can be described by the LSW theory:[18]

$$\frac{d(x_{1,3}^3)}{dt} = \frac{64 \cdot \gamma_{SF} \cdot V_m^2 \cdot N_A \cdot D \cdot c_L^\infty}{9 k_B T} = \text{const} \qquad (7)$$

Thereby, the particle volume only depends on the surface energy $\gamma_{SF}$, the molar volume $V_m$, the diffusion coefficient $D$, the solubility of a flat surface $c_L^\infty$, and the temperature $T$. $N_A$ is Avogadro's constant, and $k_B$ is the Boltzmann factor. Thus, the ripening rates of the linear regions can be calculated from the slopes of Figure 8b. The nonlinear behavior for small particle sizes and increased temperatures is not considered for these calculations. The reasons for this are that, on the one hand, the approximation of the Gibbs−Thomson equation becomes more invalid with decreasing particle size. On the other hand, recent studies of Viswanatha *et al.* proposed a deviation of the diffusion-controlled growth within these regions due to counterions being adsorbed at the particle surface[19] or due to reaction controlled growth.[20] The derived ripening rates calculated from the slope of the linear regimes are shown in Figure 9. The absolute values agree with literature values for ripening rates of ZnO in ethanol at the given temperatures.[21] Evaluating the data with an Arrhenius law, we describe the temperature-dependent ripening rate as follows:

$$\frac{d(x_{1,3}^3)}{dt} = 3 \times 10^{-20} \frac{\text{nm}^3}{\text{h}} \cdot \exp\left(-\frac{E_A}{RT}\right) \qquad (8)$$

with an activation enthalpy for ripening of 116 kJ/mol. This value is higher than the literature value of 38 kJ/mol reported by Oskam *et al.*[7] for the ripening of ZnO precipitated with NaOH in 2-propanol. Hu *et al.*[21] showed that the used solvent has a strong influence on the ripening kinetics, and recent results of Viswanatha *et al.*[19] showed that $Na^+$ ions strongly inhibit the particle growth. In contrast, Meulenkamp[8] found an increased growth kinetic in the presence of $Li^+$. Thus, the deviation in the activation enthalpy may arise from different affinities of the different cations to the nanoparticle surface as we use LiOH for the ZnO precipitation.

Beside the activation enthalpy, the temperature-dependent surface energies and mean solubilities of a large ZnO crystal are determined. For this purpose, the surface energy of eq 7 is coupled with a prefactor of 0.414 according to Mersmann[22] and the diffusion coef-

ficient is expressed *via* the Stokes−Einstein equation:

$$\frac{d(x_{1,3}^{3})}{dt} = 0.98\frac{V_m \cdot N_A \cdot k_B T \cdot c_L^{\infty}}{\pi \cdot \eta_f} \cdot \ln \frac{\rho_P}{M \cdot c_L^{\infty}} \quad (9)$$

Thus the ripening rate only depends on the global solubility $c_L^{\infty}$ of an infinitely large crystal and can be calculated analytically from the experimentally determined ripening rates. The surface energy is determined according to Mersmann from material specific parameters:

$$\gamma_{SF} = 0.414 \cdot \frac{k_B T}{\sqrt[3]{V_m^2}} \cdot \ln \frac{\rho_s}{c_L^{\infty} \cdot M} \quad (10)$$

The determined values for the surface energy and the mean solubility are shown in Figure 10. The solubility increases betwe10en 10 and 50 °C by 2 orders of magnitude from $1.7 \times 10^{-13}$ to $2.5 \times 10^{-11}$ mol/L (Figure 10a), whereas the surface energy decreases from 0.64 to 0.62 J/m$^2$ (Figure b). Compared to the literature, where theoretically estimated surface energies of macroscopic ZnO between 0.1 and 0.7 J/m$^2$ have been reported,[23−25] the values are quite reasonable. Our approach does not consider adsorption of ions at the particle surface. This effect might be included in the next step by modeling the surface energy based on the Gibbs adsorption isotherm as it was done in the case of barium sulfate in water.[26,27]

## CONCLUSION

An algorithm for the calculation of PSDs of ZnO nanoparticles was developed. This method decomposes the measured absorbance spectrum into contributions of narrow size fractions. It is based on literature values for the complex dielectric function of the bulk phase determined by ellipsometry and correlates the measurement wavelengths with particle sizes by a TBM approximation. The distinct contributions of the different particle size fractions are obtained by decomposing the measured spectrum stepwise from the largest to the smaller wavelengths. The model was validated by comparing the calculated PSD with the results of TEM image analysis and by the analysis of bimodal distributions formed by mixing the suspensions with varying volume fractions. Additionally, the algorithm was extended to the calculation of the particle solid concentration by including a size-dependent mean extinction coefficient $\varepsilon$ in the calculations. The applicability of the model on the evaluation of ripening experiments is shown, and unknown material properties, such as the mean solubility of ZnO in ethanol at different temperatures and the corresponding surface energies, are derived without prior assumption of either value. However, our model is not limited to ripening experiments but also applicable to the evaluation of transient nucleation and growth kinetics using an absorbance spectrophotometer that is present in most laboratories and is comparatively cheap. These are key parameters with regard to forming an understanding of the still unclear mechanisms of ZnO particle formation. In addition, using our algorithm and given availability of bulk absorbance data and small, nonscattering particles, it is possible to derive PSDs from the absorbance spectra of other semiconductor material systems. The evaluation of the ripening and growth kinetics allows the determination of so far mostly unknown properties of nanoparticles including size-dependent solubility, surface energy, and activation energy.

## EXPERIMENTAL SECTION

Ethyl alcohol (99.98%, VWR, Germany) was used for the preparation of all educt solutions. A 0.1 M zinc acetate dihydrate (ACS grade, 98.0−101.0%, VWR, Germany) precursor stock solution was prepared and mixed with an equimolar amount of lithium hydroxide (98%, VWR, Germany) at 20 °C, resulting in instantaneous particle formation. Different particle sizes were obtained due to the strong temperature influence on the ripening behavior (Ostwald ripening) of ZnO[6−8,21] by storing one-half of an as-prepared ZnO suspension 3 days at −10 °C and one-half of the same suspension at 20 °C.

Absorbance spectra between 250 and 400 nm were monitored using a Cary 100 scan UV−visible spectrophotometer (Varian Deutschland GmbH, Germany). DLS measurements were recorded using the Zetasizer Nano ZS (Malvern Instruments Ltd., UK), and TEM images were made on a high-resolution instrument (CM 300 LaB6/Ultratwin, Philips). Images (~50 particles) were analyzed manually using the software Axio Vision (Carl Zeiss Jena, Germany) with the diameter of a circle of equivalent area to that of the measured particle being used as the particle size. Neither washing nor any other postprocessing of the suspensions was performed.

*Acknowledgment.* The authors would like to thank the German Research Council (DFG) for their financial support (Projects PE 427/11-2 and PE 427/18-2) and for the support within the framework of its Excellence Initiative for the Cluster of Excellence "Engineering of Advanced Materials" (www.eam.uni-erlangen.de) at the University of Erlangen-Nuremberg. We thank Prof. Tim Clark for helpful discussion on quantum mechanical basis of the absorbance spectra.

## REFERENCES AND NOTES

1. Spanhel, L. Colloidal ZnO Nanostructures and Functional Coatings: A Survey. *J. Sol−Gel Sci. Technol.* **2006**, *39*, 7–24.
2. Klingshirn, C. ZnO: From Basics towards Applications. *Phys. Status Solidi B* **2007**, *244*, 3027–3073.
3. Segets, D.; Martinez Tomalino, L.; Gradl, J.; Peukert, W. Real-Time Monitoring of the Nucleation and Growth of ZnO Nanoparticles Using an Optical Hyper-Rayleigh Scattering Method. *J. Phys. Chem. C* **2009**, accepted.
4. Marczak, R.; Werner, F.; Gnichwitz, J. F.; Hirsch, A.; Guldi, D. M.; Peukert, W. Communication *via* Electron and Energy Transfer between Zinc Oxide Nanoparticles and Organic Adsorbates. *J. Phys. Chem. C* **2009**, *113*, 4669–4678.
5. Bawendi, M. G.; Steigerwald, M. L.; Brus, L. E. The Quantum Mechanics of Larger Semiconductor Clusters ("Quantum Dots"). *Annu. Rev. Phys. Chem.* **1990**, *41*, 477–496.

6. Wong, E. M.; Bonevich, J. E.; Searson, P. C. Growth Kinetics of Nanocrystalline ZnO Particles from Colloidal Suspensions. *J. Phys. Chem. B* **1998**, *102*, 7770–7775.
7. Oskam, G.; Hu, Z.; Penn, R. L.; Pesika, N.; Searson, P. C. Coarsening of Metal Oxide Nanoparticles. *Phys. Rev. E* **2002**, *66*, 11403/1–11403/4.
8. Meulenkamp, E. A. Synthesis and Growth of ZnO Nanoparticles. *J. Phys. Chem. B* **1998**, *102*, 5566–5572.
9. Ratkovich, A. S.; Penn, R. L. Controlling Nanosized ZnO Growth Kinetics Using Various Zn:OH Concentration Ratios. *J. Phys. Chem. C* **2007**, *111*, 14098–14104.
10. Ratkovich, A. S.; Penn, R. L. Controlling Oriented Aggregation Using Increasing Reagent Concentrations and Trihalo Acetic Acid Surfactants. *J. Solid State Chem.* **2008**, *181*, 1600–1608.
11. Brus, L. E. Electron−Electron and Electron−Hole Interactions in Small Semiconductor Crystallites: The Size Dependence of the Lowest Excited Electronic State. *J. Chem. Phys.* **1984**, *80*, 4403–4409.
12. Viswanatha, R.; Sapra, S.; Satpati, B.; Satyam, P. V.; Dev, B. N.; Sarma, D. D. Understanding the Quantum Size Effects in ZnO Nanocrystals. *J. Mater. Chem.* **2004**, *14*, 661–668.
13. Pesika, N. S.; Stebe, K. J.; Searson, P. C. Relationship between Absorbance Spectra and Particle Size Distributions for Quantum-Sized Nanocrystals. *J. Phys. Chem. B* **2003**, *107*, 10412–10415.
14. Yoshikawa, H.; Adachi, S. Optical Constants of ZnO. *Jpn. J. Appl. Phys.* **1997**, *36*, 6237–6243.
15. Bergström, L.; Meurk, A.; Arwin, H.; Rowcliffe, D. J. Estimation of Hamaker Constants of Ceramic Materials from Optical Data Using Lifshitz Theory. *J. Am. Ceram. Soc.* **1996**, *79*, 339–348.
16. Kim, C. G.; Sung, K.; Chung, T.-M.; Jung, D. Y.; Kim, Y. Monodispersed ZnO Nanoparticles from a Single Molecular Precursor. *Chem. Commun.* **2003**, 2068–2069.
17. Wagner, C. Theorie der Alterung von Niederschlägen durch Umlösen. *Z. Elektrochem.* **1961**, *65*, 581–591.
18. Lifshitz, I. M.; Sloyzov, V. V. The Kinetics of Precipitation from Supersaturated Solid Solutions. *J. Chem. Phys.* **1961**, *19*, 35–50.
19. Viswanatha, R.; Amenitsch, H.; Sarma, D. D. Growth Kinetics of ZnO Nanocrystals: A Few Surprises. *J. Am. Chem. Soc.* **2007**, *129*, 4470–4475.
20. Viswanatha, R.; Santra, P. K.; Dasgupta, C.; Sarma, D. D. Growth Mechanism of Nanocrystals in Solution: ZnO, a Case Study. *Phys. Rev. Lett.* **2007**, *98*, 255501/1–255501/4.
21. Hu, Z.; Oskam, G.; Searson, P. C. Influence of the Solvent on the Growth of ZnO Nanoparticles. *J. Colloid Interface Sci.* **2003**, *263*, 454–460.
22. Mersmann, A. Calculation of Interfacial Tensions. *J. Cryst. Growth* **1990**, *102*, 841–847.
23. Solomon, A. A.; Hsu, F. Swelling and Gas Release in ZnO. *J. Am. Ceram. Soc.* **1980**, *63*, 467–474.
24. Zangwill, A. *Physics at Surfaces*; Cambridge University Press: Cambridge, 1988.
25. Li, J. G. Some Observations on Wetting in the $Bi_2O_3$−ZnO System. *J. Mater. Sci. Lett.* **1994**, *13*, 400–403.
26. Schwarzer, H. C.; Schertfirm, F.; Manhart, M.; Schmid, H. J.; Peukert, W. Predictive Simulation of Nanoparticle Precipitation Based on the Population Balance Equation. *Chem. Eng. Sci.* **2006**, *61*, 167–181.
27. Schwarzer, H. C.; Peukert, W. Tailoring Particle Size through Nanoparticle Precipitation. *Chem. Eng. Commun.* **2004**, *191*, 580–606.